CrossMark

Influence of porosity on the flexural and vibration response of gradient plate using nonpolynomial higher-order shear and normal deformation theory

Ankit Gupta · **Mohammad Talha**

Abstract The present article deals with flexural and vibration response of functionally graded plates with porosity. The basic formulation is based on the recently developed non-polynomial higher-order shear and normal deformation theory by the authors'. The present theory contains only four unknowns and also accommodate the thickness stretching effect. The effective material properties at each point are determined by two micromechanics models (Voigt and Mori–Tanaka scheme). The governing equations for FGM plates are derived using variational approach. Results have been obtained by employing a C^0 continuous isoparametric Lagrangian finite element with eight degrees of freedom per node. Convergence and comparative study with the reported results in the literature, confirm the accuracy and efficiency of the present model and finite element formulation. The influence of the porosity, various boundary conditions, geometrical configuration and micromechanics models on the flexural and vibration behavior of FGM plates is examined.

Keywords Porosity · Nonpolynomial higher-order shear and normal deformation theory · Flexural · Vibration · Voigt · Mori–Tanaka

A. Gupta (✉) · M. Talha
School of Engineering, Indian Institute of Technology
Mandi, Mandi, Himachal Pradesh 175005, India
e-mail: erankit04@gmail.com

1 Introduction

Over the last three decades, composite materials, have been the dominant emerging materials. The diversified applications of composite materials have grown steadily, penetrating and conquering new markets persistently. Further, the need of composite for the structural application has placed a high emphasis on the use of new and advanced materials which can be tailored microstructurally as per the requirement. Functionally graded materials (FGMs) are also a class of composites that have a continuous variation of material properties from one surface to another (Gupta et al. 2015). The gradation of properties in an FGM reduces the thermal stresses, residual stresses, and stress concentrations found in conventional composites.

Prediction of the realistic response of any structural component depends on its structural kinematics. In this regard, first plate theory was proposed by Kirchhoff (1850), known as Classical plate theory (CPT). This theory does not include transverse shear and normal stress hence, delivers irrational results for the thick plate. To conquer this limitation, displacement and stress based first order shear deformation theory (FSDT) was proposed by Mindlin (1951) and Reissner (1945) respectively. In FSDT, the shear correction factor is used to define the proper shear stress distribution. Its value depends on the geometric and loading conditions of the structure. To avoid

restriction associated with CPT and FSDT, several higher-order shear deformation theories (HSDT) have been proposed in the last two decades. In this framework, research carried out by Basset (1890), Lo et al. (1977), Levinson (1980), Murthy (1981), Kant et al. (1982) and Reddy (1984), can be treated as a benchmark in polynomial higher-order shear deformation theory. These polynomial HSDT used Taylor series coefficients to include the shear deformation. Therefore, these are relatively complex and computationally expensive.

To circumvent the aforesaid limitations, nonpolynomial higher-order shear deformation theories have been developed in which shear strain function is used to demonstrate the shear deformation. Touratier (1991), Soldatos (1992) and Karama et al. (2009) employed sinusoidal, sinusoidal hyperbolic and exponential shear strain function respectively. Recently, Mantari (2012) investigated the flexural response of FGM plate using new sinusoidal function based HSDT with five unknowns. Thai and Choi (2013) presented cubic, sinusoidal, hyperbolic, and exponential function based HSDT to study the static and vibration response of FGM plate. Authors divided the transverse displacement in the bending and shear component to reduce the number of unknowns. Belabed et al. (2014) proposed hyperbolic function based higher-order shear deformation theory with five unknowns to investigate flexural and vibration characteristics of FGM plate. Ameur et al. (2011) showed the closed form solution to investigate the bending response of FGM plate using trigonometric shear deformation theory with four unknowns. Atmane et al. (2010) developed a new higher shear deformation theory to investigate the free vibration analysis of simply supported functionally graded plates resting on a Winkler–Pasternak elastic foundation. Nguyen (2015) presented the closed form solution of static, vibration and buckling response of FGM plate using hyperbolic higher-order shear deformation theory with four unknowns. Zenkour (2005) presented the sinusoidal shear deformation plate theory to study buckling and free vibration of simply supported FG plates. Thai and Kim (2013) presented quasi-3D sinusoidal shear deformation theory with only five unknowns for bending behavior of simply supported FGM plates. The closed form solution of free vibration response of FGM plate using four-variable refined plate theory was given by Hadji et al. (2011).

Apart from the development of such theories, several kinds of literature are available in which implementation of these theories along with 3D exact solution are given to investigate static and dynamic characteristics of the composite plate. In this framework, Reddy (2000) proposed a finite element model based on the third-order deformation theory to investigate the static and dynamic responses of FGM plate under mechanical and thermal loading. Pandya and Kant (1988) presented isoperimetric finite element formulation to investigate the static response of advanced composite plate. The flexural response of the FGM plate using collocation multiquadric radial basis functions is investigated by Ferreira et al. (2005). Wu et al. (2010) developed a modified Pagano method for three-dimensional (3-D) analysis of simply-supported, functionally graded rectangular plates under magneto-electro-mechanical loads. Jha et al. (2013) presented a free vibration response of FG elastic, rectangular, and simply supported plates based on polynomial higher order shear/shear-normal deformations theories. Alipour et al. (2010) presented a semi-analytical solution to study the vibration response of two-directional-functionally graded circular plates, resting on elastic foundations. Authors implemented Mindlin's plate theory and the differential transformation technique to obtain the governing equations of motion. Kashtalyan (2004) presented the 3D elasticity solution for the flexural response of FGM plates, in which Young's modulus of the plate is assumed to vary exponentially through the thickness coordinate. Lal et al. (2012) used Reddy's third-order shear deformation theory to investigate the nonlinear bending response of FGM plate with random material properties. Prakash and Ganapathi (2006) used three-noded shear flexible plate element based on the field-consistency principle to study the free vibration and thermos-elastic buckling characteristics of circular FGM plates.

Talha and Singh (2010) investigated the static response and free vibration analysis of FGM plates using higher-order shear deformation theory with a special modification in the transverse displacement. Gupta et al. (2016a, b) used the polynomial higher order shear and normal deformation theory with 13DOF to analyze the vibration characteristics of FGM plate. Matsunaga (2009) presented Navier solution in the conjunction of two-dimensional higher-order theory to examine the flexural response

of FGM plate under thermal and mechanical loads. The free vibration analysis of plates made of FGMs with an arbitrary gradient was carried out by Benachour et al. (2011) using a four-variable refined plate theory. Mantari and Soares (2013) examined the bending response of FGM plates by using a new trigonometric higher order and hybrid quasi-3D shear deformation theories.

Mojdehi et al. (2011) presented the 3D elastic solution of FGM plates based on the MLPG method and MLS approximation. Authors found that the centroidal deflection of FGM plates lies in between those of a pure ceramic and a pure metallic plate for both static and dynamic loads. Xiang and Kang (2013) used a meshless method based on thin plate spline radial basis function for the flexural response of FGM plates based on various higher-order shear deformation theories. Qian et al. (2004) studied the static and dynamic deformation of thick functionally graded elastic plates by using higher order shear and normal deformable plate theories and meshless local Petrov–Galerkin method. Zenkour (2006) presented generalized shear deformation theory for the static response of FGM plates. Effective material properties were calculated by assuming a power-law. The comparative study of the effect of various gradation laws (power-law, sigmoid or exponential function) on the mechanical behavior of FGM plates under transverse load was carried out by Chi and Chung (2006). Vaghefi et al. (2010) showed a three-dimensional solution for thick FGM plates by utilizing a meshless Petrov–Galerkin method. An exponential function was assumed for the variation of Young's modulus through the thickness of the plate. Tamijani and Kapania (2012) used FSDT with element free Galerkin method to study the free vibration of an FG plate with curvilinear stiffeners. Zhu and Liew (2011) presented free vibration analyses of metal and ceramic FG plates with the local Kriging meshless method.

In addition, it is found from the literature (Ebrahimi and Zia 2015; Atmane et al. 2015) that during the fabrication process of FGMs, some microstructural defects i.e. micro-voids or porosities can accrue in the materials due to the large difference in solidification temperatures between the constituent materials. Wattanasakulpong and Ungbhakorn (2014), Wattanasakulpong et al. (2012) highlighted on the existence of porosities inside the FGM during multistep sequential infiltration fabrication process. Therefore, it necessitates to include the porosity effect during computing the effective material properties of FGM plate. There are only a few reports available in the open literature dealing with the vibration and flexural analysis of FGM plate with porosity. Yahia et al. (2015) used higher-order shear deformation theories to study the wave propagation of an infinite FGM plate with porosities. The linear and nonlinear dynamic stability of a circular porous plate has been investigated to determine the critical loads in two separate studies by Magnucka-Blandzi (2010). Moreover, Mechab et al. (2016) have developed a nonlocal elasticity model for vibration of nanoplates made of porous FG material resting on elastic foundations.

Koiter (1959) and Carrrera et al. (2011) emphasized on the importance of thickness stretching effect on the structural response of the composite structure. From the aforesaid review, it is observed that most of the HSDT do not accommodate transverse normal strain which leads to the negligence of thickness stretching effect. It is also found that the available literature for the vibration and flexural response of FGM plates with porosity are relatively scarce. Therefore, the objective of the present work is set to investigate the flexural and vibration analysis of FGM plates with porosity using recently developed non-polynomial based higher-order shear and normal deformation theory by the authors' (Gupta and Talha 2016; Gupta et al. 2017). The present theory consists of a nonlinear variation of in-plane and transverse displacement along the thickness direction and also accommodate the thickness stretching effect. The effective material properties of FGM plate with porosity are computed using newly proposed model. To implement this theory, a suitable C^0 continuous isoparametric finite element with eight degrees of freedom (DOFs) per node is considered to minimize the computational complicacy. In order to compute the graded material properties, two micromechanics model (Voigt and Mori–Tanaka) is used with the conjunction of the power law. The influence of porosity volume fraction, volume fraction index, geometric configurations, and various boundary constraints on the flexural and vibration characteristics of FGM plates is investigated.

2 Mathematical formulation

The mathematical formulation of the actual physical problem of the FGM plates subjected to mechanical

loading is presented. An FGM plate with porosity having thickness 'h', length 'a', and width 'b' is considered and is shown in Fig. 1.

2.1 Constitutive equations and material properties

The Voigt model and Mori–Tanaka are used in the present study to compute the effective material properties of FGM plate.

2.1.1 Mori–Tanaka model

According to the Mori–Tanaka scheme (Mori 1973), the effective Young's modulus E_f and Poisson's ratio v_f can be calculated using effective bulk modulus (K_f) and shear modulus (G_f) of the FGM plate as

$$\frac{K_f(z) - K_c}{K_m - K_c} = \frac{V_m}{1 + [1 - V_m]\frac{3[K_m+K_c]}{[3K_c+4G_c]}}$$
$$\frac{G_f(z) - G_c}{G_m - G_c} = \frac{G_f(z)}{1 + [1 - V_m]\left(\frac{G_m+G_c}{G_c+f_1}\right)} \quad (1)$$

where, $f_1 = \frac{G_c[9K_c+8G_c]}{[6K_c+2G_c]}$ and K_c, G_c, K_m and G_m are the bulk modulus and shear modulus of ceramic and metal respectively. From Eq. (1), the effective material properties are represented as

$$E_f(z) = \frac{9K_f(z)G_f(z)}{3K_f(z) + G_f(z)}, \quad v_f(z) = \frac{3K_f(z) - 2G_f(z)}{6K_f(z) + 2G_f(z)} \quad (2)$$

2.1.2 Voigt model

The Voigt model is simple and has been adopted in most of the analyses of FGM structures (Gibson 1995). The effective material properties(p_e) in a specific direction (along with 'z') is determined by

$$V_m + V_c = 1$$
$$p_e = (p_c - p_m)V_c + p_m \quad (3)$$

where, 'p_e' represents the effective material property (Young's modulus, mass density, Poisson's ratio), subscripts m and c represents the metallic and ceramic constituents, respectively. The volume fraction V_c is assumed to follow a simple power law in both the model as

$$V_c = \left(\frac{z}{h} + \frac{1}{2}\right)^n \quad (4)$$

where 'n' is the volume fraction index. To incorporate the porosity, a new mathematical expression is modeled with the help of slight modification in the

Fig. 1 The geometric configuration of FGM Plate with porosity
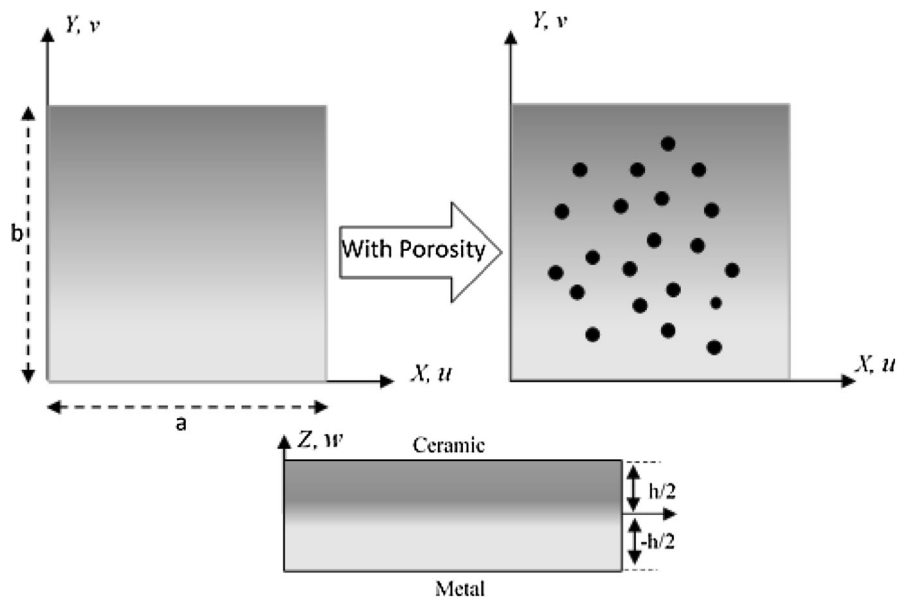
rule of mixture as given in Eq. (3). The material properties with porosity are anticipated to follow the power law in the present study and are expressed as

$$P = P_c(V_c - \log(1 + \lambda/2)) + P_m(V_m - \log(1 + \lambda/2)) \quad (5)$$

'λ' is termed as porosity volume fraction ($\lambda < 1$). $\lambda = 0$ indicates the non-porous functionally graded plate. The effective material property of porous FGM plate is given as

$$E(z) = [E_c - E_m]\left(\frac{2z + h}{2z}\right)^n$$
$$- \log(1 + \lambda/2)[E_c + E_m]\left[1 - \frac{2|z|}{h}\right] + E_m$$

$$\rho(z) = [\rho_c - \rho_m]\left(\frac{2z + h}{2z}\right)^n$$
$$- \log(1 + \lambda/2)[\rho_c + \rho_m]\left[1 - \frac{2|z|}{h}\right] + \rho_m$$
$$(6)$$

The linear constitutive relations of an FG plate is given by Talha and Singh (2011):

$$\begin{Bmatrix} \sigma_{xx} \\ \sigma_{yy} \\ \sigma_{zz} \\ \tau_{yz} \\ \tau_{zx} \\ \tau_{xy} \end{Bmatrix} = \begin{bmatrix} C_{11} & C_{12} & C_{12} & 0 & 0 & 0 \\ C_{12} & C_{11} & C_{12} & 0 & 0 & 0 \\ C_{12} & C_{12} & C_{11} & 0 & 0 & 0 \\ 0 & 0 & 0 & C_{44} & 0 & 0 \\ 0 & 0 & 0 & 0 & C_{55} & 0 \\ 0 & 0 & 0 & 0 & 0 & C_{66} \end{bmatrix} \begin{Bmatrix} \varepsilon_{xx} \\ \varepsilon_{yy} \\ \varepsilon_{zz} \\ \gamma_{yz} \\ \gamma_{zx} \\ \gamma_{xy} \end{Bmatrix}$$
$$(7)$$

$C_{11} = E(z)(1 + \upsilon)/(1 - 2\upsilon)(1 + \upsilon)$
$C_{12} = \upsilon E(z)/(1 - 2\upsilon)(1 + \upsilon)$
$C_{44} = C_{55} = C_{66} = E(z)/2(1 + \upsilon)$

2.2 Displacement fields

A recently developed non-polynomial based higher-order shear and normal deformation theory by the authors' Gupta and Talha (2016), Gupta et al. (2017) is considered to investigate the realistic flexural and vibration responses of the porous graded plates as given in Eq. (8):

$$\bar{u}(x, y, z, t) = u_o(x, y, t) - z\left(\frac{\partial w_b}{\partial x}\right)$$
$$- \psi\left[\sinh^{-1}\left(\frac{\kappa z}{h}\right) - \left(\frac{\kappa}{h}\right)z\right]\frac{\partial w_s}{\partial x}$$

$$\bar{v}(x, y, z, t) = v_o(x, y, t) - z\left(\frac{\partial w_b}{\partial y}\right)$$
$$- \psi\left[\sinh^{-1}\left(\frac{\kappa z}{h}\right) - \left(\frac{\kappa}{h}\right)z\right]\frac{\partial w_s}{\partial y}$$

$$\bar{w}(x, y, z, t) = w_b(x, y, t) + \kappa\cosh^2\left(\frac{\kappa z}{h}\right)w_s(x, y, t)$$

Here, $\psi = -\dfrac{h\cosh^2(\kappa/2)}{\sqrt{(1 + \kappa^2/4)} - 1}$ (8)

where $\bar{u}$, $\bar{v}$ and $\bar{w}$ signifies the displacements of a point along the (x, y, z) coordinates. u_o, v_o, w_b and w_s are the four unknown displacement functions of mid-plane. The value of shape parameter 'κ' is deliberated in the post-processing phase and is evaluated as 3.4.

2.3 Strain–displacement relations

The non-zero linear strains associated with the displacement field in Eq. (8) is represented as,

$$\{\boldsymbol{\varepsilon}\}_{6x1} = [\mathfrak{M}]_{6x16}\{\bar{\varepsilon}\}_{16x1} \quad (9)$$

where $\{\bar{\varepsilon}\}_{16x1}$ are the components of generalized strains. The non-zero strains are given below,

$$\begin{Bmatrix} \varepsilon_{xx} \\ \varepsilon_{yy} \\ \varepsilon_{zz} \\ \gamma_{xy} \\ \gamma_{xz} \\ \gamma_{yz} \end{Bmatrix} = \begin{Bmatrix} \varepsilon_{xx}^0 \\ \varepsilon_{yy}^0 \\ \varepsilon_{zz}^0 \\ \gamma_{xy}^0 \\ \gamma_{xz}^0 \\ \gamma_{yz}^0 \end{Bmatrix} + z\begin{Bmatrix} \varepsilon_{xx}^1 \\ \varepsilon_{yy}^1 \\ 0 \\ \gamma_{xy}^1 \\ 0 \\ 0 \end{Bmatrix} + f(z)\begin{Bmatrix} \varepsilon_{xx}^2 \\ \varepsilon_{yy}^2 \\ 0 \\ \gamma_{xy}^2 \\ 0 \\ 0 \end{Bmatrix}$$
$$+ \phi(z)\begin{Bmatrix} 0 \\ 0 \\ 0 \\ 0 \\ \gamma_{xz}^1 \\ \gamma_{yz}^1 \end{Bmatrix} + g(z)\begin{Bmatrix} 0 \\ 0 \\ 0 \\ 0 \\ \gamma_{xz}^2 \\ \gamma_{yz}^2 \end{Bmatrix} \quad (10)$$

where, $f(z) = \psi\left[\sinh^{-1}\left(\frac{\kappa z}{h}\right) - \left(\frac{\kappa}{h}\right)z\right]$, $g(z) = \kappa\cosh^2\left(\frac{\kappa z}{h}\right)$, $\phi(z) = g'(z)$, $\varepsilon_{xx}^0 = \frac{\partial u_0}{\partial x}$, $\varepsilon_{yy}^0 = \frac{\partial v_0}{\partial y}$, $\varepsilon_{zz}^0 = (2\kappa^2/h)w_s\cosh\left(\frac{\kappa z}{h}\right)\sinh\left(\frac{\kappa z}{h}\right)$, $\gamma_{xz}^0 = -\left(\frac{\kappa\psi}{h}\right)\frac{\partial w_s}{\partial x}$, $\gamma_{xz}^1 = \kappa\psi h$,

$\gamma_{xz}^2 = \kappa \frac{\partial w_s}{\partial x}. \ \gamma_{yz}^0 = -\frac{\kappa \psi}{h} \frac{\partial w_s}{\partial y}, \ \gamma_{yz}^1 = \kappa \psi h, \ \gamma_{yz}^2 = \kappa \frac{\partial w_s}{\partial y},$

$\gamma_{xy}^0 = \frac{\partial u_0}{\partial y} + \frac{\partial v_0}{\partial x}, \ \gamma_{xy}^1 = -\frac{\partial^2 w_b}{\partial x \partial y} - \frac{\kappa \psi}{h} \frac{\partial^2 w_s}{\partial x \partial y} - \frac{\partial^2 w_b}{\partial x \partial y} - \frac{\kappa \psi}{h} \frac{\partial^2 w_s}{\partial x \partial y},$

$\gamma_{xy}^2 = 2\psi \frac{\partial^2 w_s}{\partial x \partial y} \ \varepsilon_{xx}^1 = -\frac{\partial^2 w_b}{\partial x^2} - \left(\frac{\kappa \psi}{h}\right) \frac{\partial^2 w_s}{\partial x^2}, \ \varepsilon_{yy}^1 = -\frac{\partial^2 w_b}{\partial y^2}$

$-\left(\frac{\kappa \psi}{h}\right) \frac{\partial^2 w_b}{\partial y^2}, \ \varepsilon_{xx}^2 = \psi \frac{\partial^2 w_s}{\partial x^2}, \ \varepsilon_{yy}^2 = \psi \frac{\partial^2 w_s}{\partial y^2}$

3 Solution methodology (finite element formulation)

3.1 Element selection

In the present finite element formulation, a C^0-continuous nine nodded isoparametric finite element with eight degrees of freedom per node (Fig. 2) is employed to discretize the plate geometry. Later, the generalized displacement vector and element geometry of the model at any point can be expressed in terms of shape functions as follows,

$$\{\Re\} = \sum_{i=1}^{nn} N_i \{\Re\}_i, x = \sum_{i=1}^{nn} N_i x_i, y = \sum_{i=1}^{nn} N_i y_i \quad (11)$$

where $\{N_i\}$ and $\{\Re_i\}$ are the shape function and displacement vector of ith node respectively. 'nn' is the number of nodes per element and x_i, and y_i are the Cartesian coordinate of the ith node. The shape functions at an ith node of the nine nodded elements are given as:

$$N_i = \begin{cases} \frac{1}{4} (\xi^2 + \xi_i \xi)(\eta^2 + \eta_i \eta), \ for \ i = 1, 2, 3, 4 \\ \frac{1}{2} (1 - \xi^2)(\eta^2 + \eta_i \eta), \ for \ i = 5, 7 \\ \frac{1}{2} (\xi^2 + \xi_i \xi)(1 - \eta^2), \ for \ i = 6, 8 \\ \frac{1}{2} (1 - \xi^2)(1 - \eta^2), \ for \ i = 9 \end{cases}$$

(12)

3.2 Continuity obligation

It is obvious from Eq. (9), that the in-plane displacement (i.e. $\bar{u}$ and $\bar{v}$) encompass transverse displacement derivatives ($\bar{w}$), which leads to the second order derivatives in the strain vector. Hence, it requires implementing C^1 continuity in the finite element modeling.

To eradicate the intricacy accompanying with these finite elements, the displacement field has been modified to make it appropriate for C^0 continuous element. In this framework, the transverse displacement derivatives exist in Eq. (8) are replaced as $\frac{\partial w_b}{\partial x} = \alpha_x$, $\frac{\partial w_b}{\partial y} = \alpha_y$, $\frac{\partial w_s}{\partial x} = \beta_x$, $\frac{\partial w_s}{\partial y} = \beta_y$ and $w_s = \beta_z$. After incorporating these modifications in the displacement field, four DOFs with C^1 continuity given in Eq. (8) are changed into eight DOFs with C^0 continuity as shown in Eq. (13).

Fig. 2 Configuration of nine-noded finite element in natural coordinate system
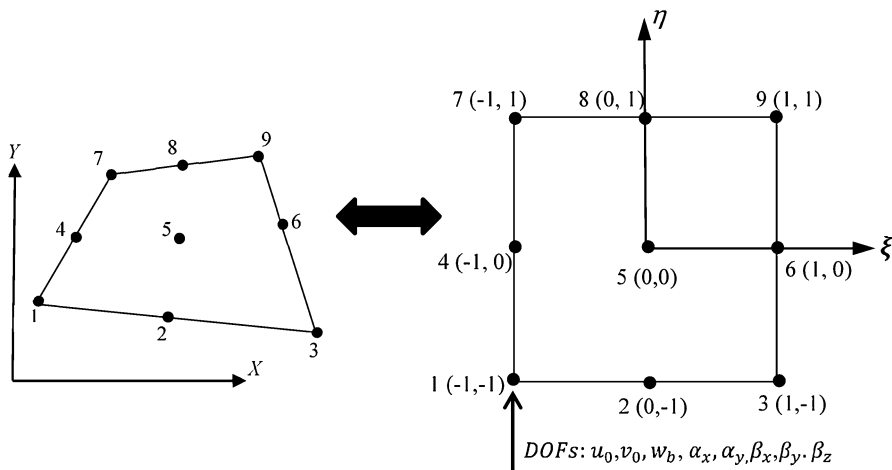
$$\bar{u}(x,y,z,t) = u_o(x,y,t) - z\left[\alpha_x + \left(\frac{\kappa\psi}{h}\right)\beta_x\right]$$
$$+ \psi\sinh^{-1}\left(\frac{\kappa z}{h}\right)\beta_x$$
$$\bar{v}(x,y,z,t) = v_o(x,y,t) - z\left[\alpha_y + \left(\frac{\kappa\psi}{h}\right)\beta_y\right]$$
$$+ \psi\sinh^{-1}\left(\frac{\kappa z}{h}\right)\beta_y$$
$$\bar{w}(x,y,z,t) = w_b(x,y,t) + \kappa\cosh^2\left(\frac{\kappa z}{h}\right)\beta_z(x,y,t) \tag{13}$$

The basic field variables can be denoted mathematically as. In this procedure, the artificial constraints are introduced which are enforced variationally through a penalty approach as given in Eq. (15).

$$\frac{\partial w_b}{\partial x} - \alpha_x = 0, \quad \frac{\partial w_b}{\partial y} - \alpha_y = 0,$$
$$\frac{\partial w_s}{\partial x} - \beta_x = 0 \text{ and } \frac{\partial w_s}{\partial y} - \beta_y = 0 \tag{14}$$

3.3 Energy equations

3.3.1 Strain energy of the plate

The strain energy of ith element of FGM plate is given by:

$$\Pi^e = \frac{1}{2}\int_V \{\boldsymbol{\varepsilon}\}_i^T\{\boldsymbol{\sigma}\}_i dV = \frac{1}{2}\int_v \{\boldsymbol{\varepsilon}\}_i^T[\boldsymbol{Q_{ij}}]\{\boldsymbol{\varepsilon_i}\}dV$$
$$= \frac{1}{2}\int_V \{\bar{\boldsymbol{\varepsilon}}\}_i^T[\mathfrak{M}]_i^T[\boldsymbol{Q_{ij}}][\mathfrak{M}]_i\{\bar{\boldsymbol{\varepsilon}}\}_i dV$$
$$= \frac{1}{2}\int_A \{\mathfrak{R}\}_i^T[\mathbf{B}]_i^T[\boldsymbol{D}][\mathbf{B}]_i\{\mathfrak{R}\}_i dA$$
$$= \frac{1}{2}\{\mathfrak{R}\}_i^T[\boldsymbol{K}]_i\{\mathfrak{R}\}_i \tag{15}$$

If 'ne' is the number of elements used for meshing the plate, the strain energy of the plate is given as,

$$\prod = \sum_{e=1}^{ne}\Pi^{(e)}, \prod = \frac{1}{2}\sum_{e=1}^{ne}\{\mathfrak{R}\}^{(e)T}[\boldsymbol{K}]^{(e)}\{\mathfrak{R}\}^{(e)} \tag{16}$$

where $[\boldsymbol{K}]^{(e)}$ and $\{\mathfrak{R}\}^{(e)}$ are the linear stiffness matrix and displacement vector for the element, respectively.

3.3.2 Kinetic energy of the plate

The kinetic energy of FGM plate is given by:

$$\Delta = \frac{1}{2}\int_V \rho\{\dot{\boldsymbol{\Lambda}}\}^T\{\dot{\boldsymbol{\Lambda}}\}dV \tag{17}$$

where 'ρ'and $\{\boldsymbol{\Lambda}\}$ are the density and global displacement vector of the plate. The global displacement field model has represented as:

$$\{\boldsymbol{\Lambda}\} = [\bar{\mathbf{N}}]\{\mathfrak{R}\} \tag{18}$$

where the matrix $[\bar{\mathbf{N}}]$ is the function of thickness coordinate which is given in "Appendix". After substituting Eq. (18) into Eq. (17), the kinetic energy of an element is obtained as:

$$\Delta^e = \frac{1}{2}\int_A \left(\int_Z \rho\{\dot{\mathfrak{R}}\}^T[\mathbf{N}]^T[\mathbf{N}]\{\dot{\mathfrak{R}}\}dz\right)dA$$
$$= \frac{1}{2}\int_A \{\dot{\mathfrak{R}}\}^T[\mathbf{M}]^{(e)}\{\dot{\mathfrak{R}}\}dA \tag{19}$$

Kinetic energy of vibrating plate for total number of element 'ne' is given as

$$\Delta = \sum_{e=1}^{ne}\Delta^{(e)} \tag{20}$$

Here $[\mathbf{M}]^{(e)}$ is the inertia matrix of the element.

3.3.3 Work done due to transverse load

The external work done on the plate by uniformly applied load q_0 may be written as $W_{ext}^{(e)} = \int_A q_0(x,y)\{\boldsymbol{w}\}dA$

For the finite element formulation, the above equation can be written as

$$W_{ext} = \sum_{e=1}^{ne}W_{ext}^{(e)} \tag{21}$$

The total potential energy due to the applied load can be written as

$$V = -W_{ext}^{(e)} = -\int_A \{\boldsymbol{\Lambda}\}^T\{\boldsymbol{\mathcal{F}}\}dA$$
$$= -\{\boldsymbol{\Lambda}\}^{(e)T}\{\boldsymbol{\mathcal{F}}\}^{(e)} \tag{22}$$
$$\{\boldsymbol{\mathcal{F}}\}^{(e)} = \{0 \quad 0 \quad Q \quad 0 \quad 0 \quad 0 \quad 0 \quad 0\}^T$$

3.4 Governing equation

The governing equation for flexural and free vibration analysis of FG plate has been obtained using the principle of virtual work (Grover et al. 2013).

$$\int_{t_1}^{t_2} (\delta L) dt = 0 \tag{23}$$

where L is termed as Lagrangian and is demarcated as $L = \Pi - (\Delta + V)$. The final governing equation can be obtained by putting all the energy equations (Eqs. 16, 20 and 22) along with the energy function Π_c because of enforced artificial constraints during the conversion of C^1 continuity to C^0 continuity. This energy function Π_c is expressed as

Table 1 Properties of the FGM components

Material	Properties		
	E (GPa)	ν	ρ (kg/m^3)
Aluminium (Al)	70	0.30	2707
Zirconia (ZrO$_2$)	151	0.30	3000
Alumina (Al$_2$O$_3$)	380	0.30	3800
Ti–6Al–4 V	105.5	0.294	4429
Silicon nitride (Si$_3$N$_4$)	327.27	0.24	2370

$$[\mathbf{K}]\{\Re\} = \{\mathcal{F}\} \tag{27}$$

4 Numerical results and discussion

In this section, the model validation and numerical analyses for the flexural and vibration response of the

$$\Pi_c = \frac{\gamma}{2} \iint \left[\begin{array}{l} \left(\frac{\partial w_b}{\partial x} - \alpha_x\right)^T \left(\frac{\partial w_b}{\partial x} - \alpha_x\right) + \left(\frac{\partial w_b}{\partial y} - \alpha_y\right)^T \left(\frac{\partial w_b}{\partial y} - \alpha_y\right) + \\ \left(\frac{\partial w_s}{\partial x} - \beta_x\right)^T \left(\frac{\partial w_s}{\partial x} - \beta_x\right) + \left(\frac{\partial w_s}{\partial y} - \beta_y\right)^T \left(\frac{\partial w_s}{\partial y} - \beta_y\right) \end{array} \right] dxdy \tag{24}$$

Using finite element approximation Π_c is represented as: $\Pi_c = \frac{\gamma}{2}\{\Re\}^T[\mathbf{K_c}]\{\Re\}$, where $[\mathbf{K_c}]$ is the stiffness matrix due to artificial constraints. After substituting theses value in Eq. (23), the governing equation is expressed as

$$\frac{1}{2} \int_{t_1}^{t_2} \delta \left[\left\{\dot{\Re}\right\}^T [\mathrm{M}]\left\{\dot{\Re}\right\} - \{\Re\}^T[\mathbf{K} + \gamma\mathbf{K_c}]\{\Re\} \right] dt = 0 \tag{25}$$

Above equations can be used to find the required governing equations for free vibration and flexural analysis by imposing the prerequisite boundary conditions as follows:

1. The generalized eigenvalue problem for free vibration of a system can be expressed as

$$[\mathrm{M}]\left\{\ddot{\Re}\right\} + [\mathbf{K} + \gamma\mathbf{K_c}]\{\Re\} = 0, \tag{26}$$

2. The generalized governing equation for flexural analysis may be expressed as

FGM plate are performed using the finite element method. A uniform 6×6 mesh of nine noded C^o continuous elements is employed. To prevent the shear locking phenomena, the reduced integration technique is used to integrate terms related to the transverse shear stress. The description of material properties used in the analysis is provided in Table 1.

4.1 Convergence and validation of the present solution

Three test examples have been solved to show the efficacy and proficiency of the present solution along with the convergence and comparison studies. The obtained results are compared with those available in the literature. The numerical results are presented in the graphical and tabular form.

Example 1 The first example is performed for Al/Al$_2$O$_3$ square FGM plates with simply supported (SSSS) boundary condition for different values of the power law index 'n'. The non-dimensional fundamental frequency ($\bar{\omega}$) obtained by present model are

Table 2 Comparison of linear frequency parameter $\left(\bar{\omega} = \omega(a^2/h)\sqrt{\rho_c/E_c}\right)$ for Al/Al$_2$O$_3$ (SSSS) FGM plate with different mesh size for $a/h = 10$

Mesh size	Volume fraction index 'n'				
	0	0.5	1	4	10
Present 2 × 2	5.9932	5.1375	4.6665	4.0139	3.7981
Present 3 × 3	5.9739	5.1274	4.6569	3.9894	3.7739
Present 4 × 4	5.8456	5.0100	4.5527	3.9247	3.7162
Present 5 × 5	5.8033	4.9672	4.5097	3.8935	3.6932
Present 6 × 6	5.7900	4.9560	4.4997	3.8846	3.6846
Belabed et al. (2014)	5.7800	4.9400	4.4900	3.8900	3.6800
% Difference	0.173	0.323	0.216	0.138	0.125
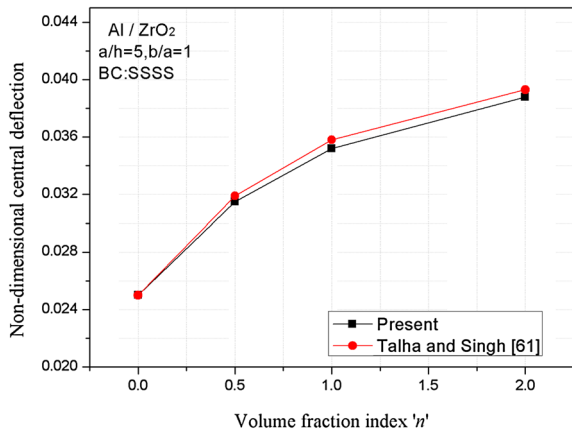
Fig. 3 Comparison of central deflection of Al/ZrO$_2$ FGM plate
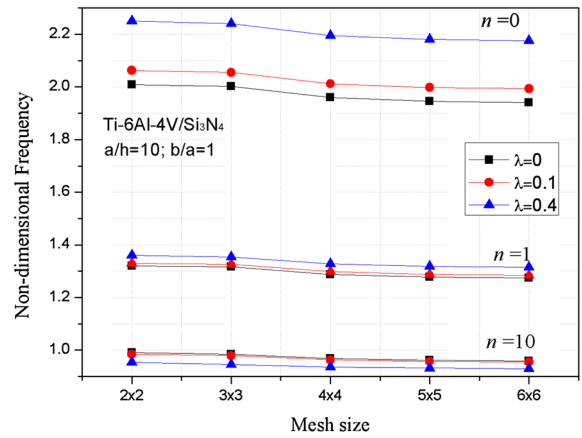
Fig. 4 Convergence for the non-dimensional frequency of FGM plate with porosity (λ: porosity volume fraction; n: volume fraction index)

compared with those given by Belabed et al. (2014) as shown in Table 2. In Ref (Belabed et al. 2014) higher-order shear and normal deformation theory with five unknowns has been used to investigate the vibration response of FGM plate. They employed Hamilton's principle to drive the governing equation of motion and frequency parameters have been calculated using Navier solution. The comparison study confirms that the present results are in excellent agreement with

Table 3 Comparison of frequency parameter of (CCCC) FGM plate (Ti–6Al–4V/Si$_3$N$_4$) for various volume fraction index 'n' and side to thickness ratio (M–T: Mori–Tanaka)

a/h	Volume fraction index 'n'									
	0		1		5		10		100	
	Voigt	M–T	Voigt	M–T	Voigt	M–T	Voigt	M–T	Voigt	M–T
5	7.6778	7.6778	5.1165	5.3330	3.9254	4.0103	3.6785	3.7331	3.2957	3.3089
10	10.0615	10.0615	6.6307	6.9037	5.2314	5.3369	4.9125	4.9938	4.3318	4.3513
20	11.0479	11.0479	7.2541	7.5461	5.8022	5.9159	5.4520	5.5476	4.7650	4.7880
30	11.3494	11.3494	7.4461	7.7440	5.9750	6.0914	5.6152	5.7150	4.8973	4.9213
50	11.5843	11.5843	7.5942	7.8964	6.1100	6.2283	5.7433	5.8463	5.0007	5.0256
100	11.7264	11.7264	7.6821	7.9866	6.1939	6.3130	5.8234	5.9285	5.0638	5.0893

Table 4 Comparison of frequency parameter of (SCSC) FGM plate (Ti–6Al–4V/Si$_3$N$_4$) for various volume fraction index 'n' and side to thickness ratio (M–T: Mori–Tanaka)

a/h	Volume fraction index 'n'									
	0		1		5		10		100	
	Voigt	M–T	Voigt	M–T	Voigt	M–T	Voigt	M–T	Voigt	M–T
5	6.3552	6.3552	4.3504	4.5337	3.3534	3.4277	3.0895	3.1554	2.7165	2.7260
10	8.2164	8.2164	5.4095	5.6308	4.2842	4.3698	4.0239	4.0915	3.5394	3.5557
20	8.8674	8.8674	5.8200	6.0533	4.6634	4.7544	4.3824	4.4598	3.8257	3.8443
30	9.0593	9.0593	5.9421	6.1792	4.7737	4.8664	4.4865	4.5666	3.9099	3.9292
50	9.2072	9.2072	6.0354	6.2752	4.8588	4.9528	4.5673	4.6494	3.9750	3.9949
100	9.2970	9.2970	6.0910	6.3322	4.9119	5.0063	4.6179	4.7014	4.0149	4.0351

Table 5 Comparison of frequency parameter of (SSSS) FGM plate (Ti–6Al–4V/Si$_3$N$_4$) for various volume fraction index 'n' and side to thickness ratio (M–T: Mori–Tanaka)

a/h	Volume fraction index 'n'									
	0		1		5		10		100	
	Voigt	M–T	Voigt	M–T	Voigt	M–T	Voigt	M–T	Voigt	M–T
5	5.1352	5.1352	3.3891	3.5271	2.6737	2.7275	2.5110	2.5523	2.2124	2.2227
10	5.7965	5.7965	3.8057	3.9581	3.0479	3.1073	2.8646	2.9149	2.5013	2.5135
20	5.9896	5.9896	3.9274	4.0834	3.1615	3.2226	2.9717	3.0251	2.5861	2.5991
30	6.0338	6.0338	3.9553	4.1120	3.1875	3.2490	2.9963	3.0504	2.6056	2.6187
50	6.0616	6.0616	3.9727	4.1299	3.2040	3.2657	3.0118	3.0664	2.6179	2.6311
100	6.0759	6.0759	3.9816	4.1390	3.2126	3.2745	3.0200	3.0749	2.6242	2.6375

those generated by Belabed et al. (2014) even though the present model consist only four unknowns. It is also clear from the convergence study that the performance of the present formulation is good in terms of solution accuracy and the rate of convergence with mesh refinement. Based on the convergence study, in the present analysis the results are obtained at (6 × 6) mesh size, and otherwise stated.

Example 2 In this example, the central deflection (w_c) of (SSSS) Al/ZrO$_2$ square FGM plates with varying volume fraction indexes (n) is computed and compared with the results given by Talha and Singh (2010). The material properties of the constituent material are $Em = 70$ GPa N/m^2, $\rho_m = 2702$ kg/m^3 for aluminium (Al), and $E_c = 151$ GPa, $\rho_c = 5700$ kg/m^3 for zirconia (ZrO$_2$). Talha and Singh (2011) used polynomial based higher-order shear deformation theory with thirteen DOF per node. It is clearly from the Fig. 3 that the solution accuracy is good for the static response for different values of volume fraction index.

Table 6 Comparison of frequency parameter of (CFSF) FGM plate (Ti–6Al–4V/Si$_3$N$_4$) for various volume fraction index 'n' and side to thickness ratio (M–T: Mori–Tanaka)

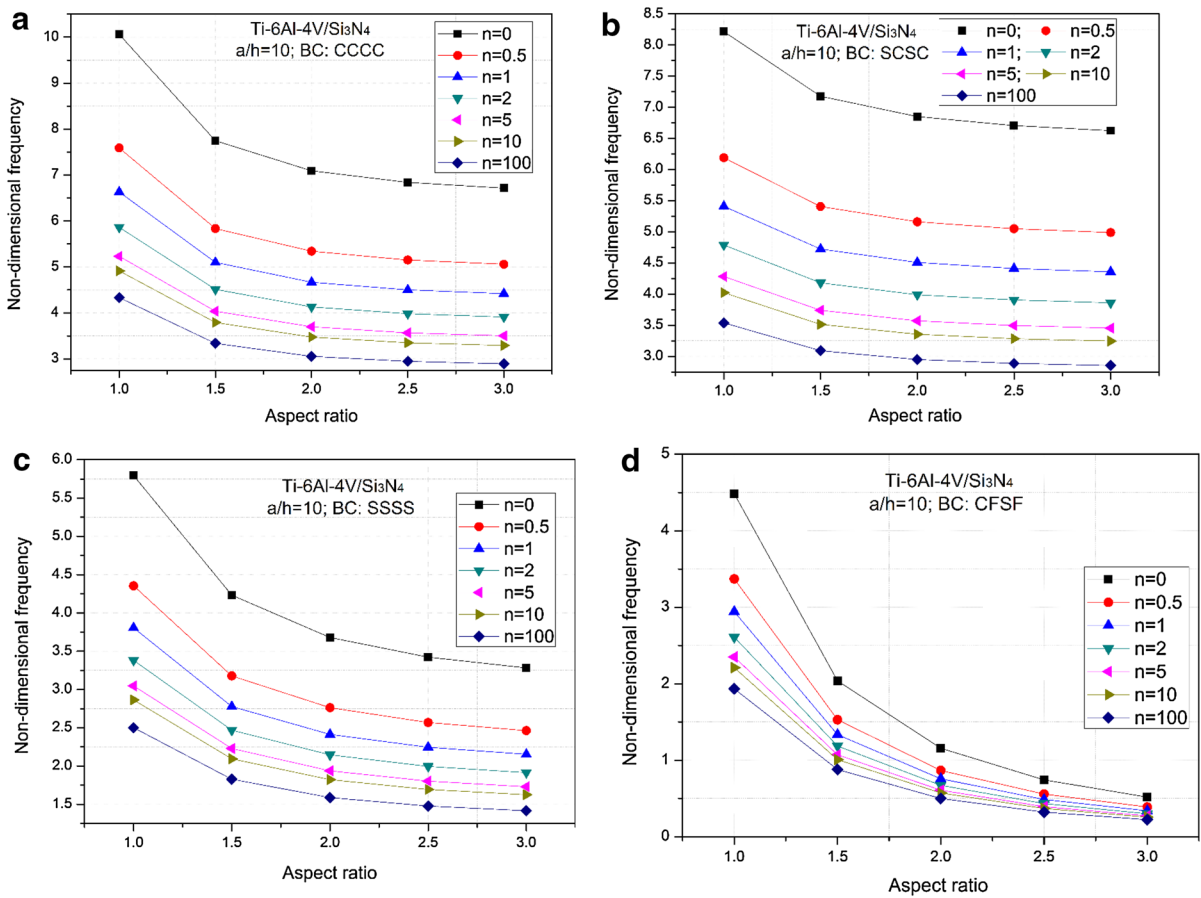| a/h	Volume fraction index 'n'									
	0		1		5		10		100	
	Voigt	M–T	Voigt	M–T	Voigt	M–T	Voigt	M–T	Voigt	M–T
5	3.9540	3.9540	2.6125	2.7213	2.0456	2.0871	1.9212	1.9516	1.7014	1.7110
10	4.4851	4.4851	2.9428	3.0618	2.3501	2.3958	2.2098	2.2478	1.9343	1.9443
20	4.6763	4.6763	3.0630	3.1855	2.4613	2.5085	2.3148	2.3557	2.0183	2.0278
30	4.7381	4.7381	3.1024	3.2262	2.4962	2.5440	2.3478	2.3895	2.0453	2.0574
50	4.7895	4.7895	3.1348	3.2595	2.5256	2.5739	2.3756	2.4180	2.0679	2.0768
100	4.8220	4.8220	3.1550	3.2802	2.5450	2.5935	2.3940	2.4370	2.0823	2.0941

Fig. 5 Non-dimensional frequency versus aspect ratio for different volume fraction index 'n'

Example 3 To verify the effectiveness of the present formulation in dealing with flexural and vibration analysis of FGM plate with porosity, a convergence study is conducted in terms of different mesh size. The analysis is performed for Simply supported Ti–6Al–4V/Si$_3$N$_4$ FGM plates having a/h ratio equals to 10 with various volume fraction indices ($n = 0$, 1 and 10). The material properties of the constituent material are $E_m = 105.7$ GPa, $\rho_m = 4429$ kg/m^3 for Ti–6Al–4V, and $E_c = 322.27$ GPa, $\rho_c = 2370$ kg/m^3 for Si$_3$N$_4$. Effective material properties of FGM plate with porosity have been calculated using the mathematical expression given in Eq. (6). The non-dimensional frequency parameter is calculated using mesh

sizes from (2×2) to (6×6) for different volume fraction indexes 'n'. It is clear from the Fig. 4 that the present solution shows the excellent convergence for the frequency parameter of FGM plate with porosity.

4.2 Parametric studies

In the view of the preceding discussion, it is observed that the present formulation delivers results which are in good agreement with various existing shear deformation theories of the FGM plate. In the subsequent section, the parametric studies have been carried out to explore the influence of various homogenization techniques, gradation rules, porosity volume fraction,
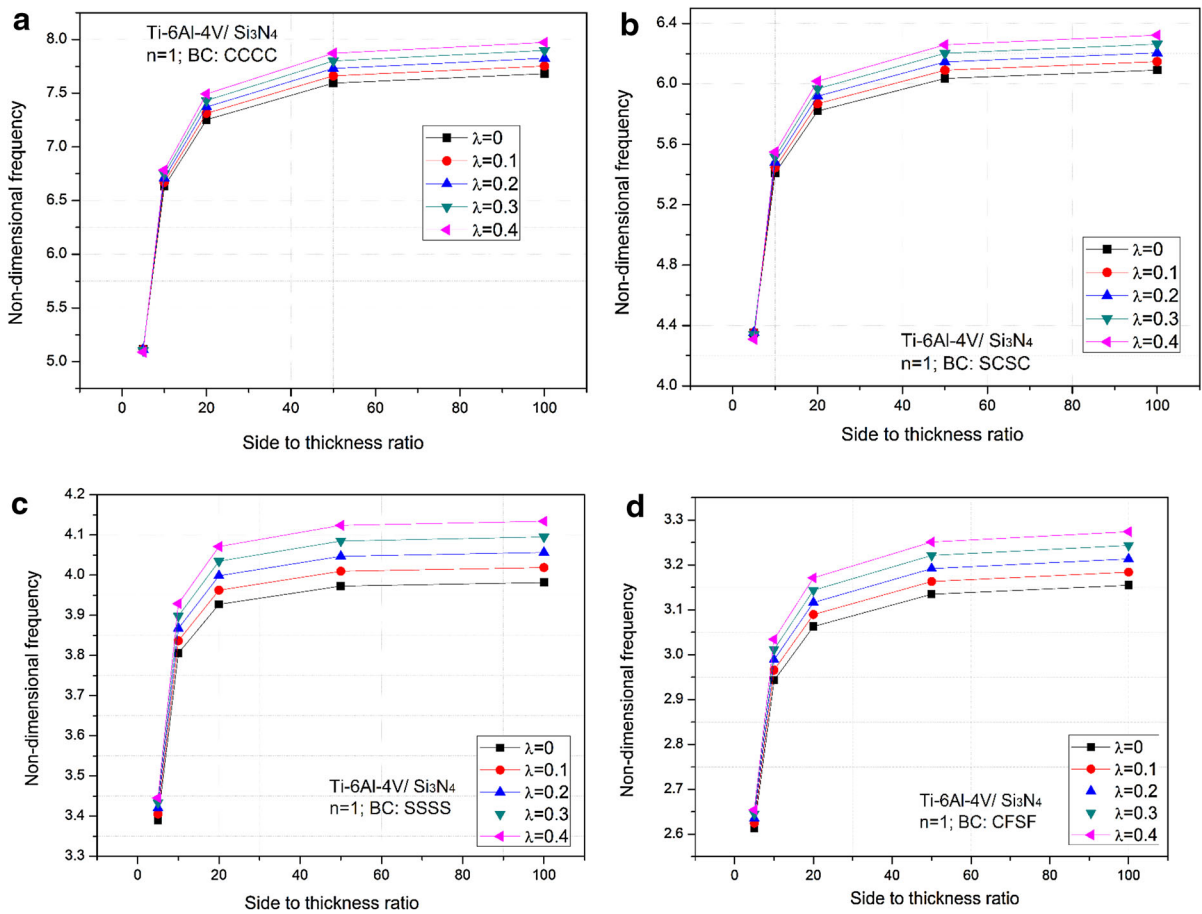
Fig. 6 Non-dimensional frequency versus side to thickness ratio for different porosity volume fraction (λ)

volume fraction index, and geometric configuration on the flexural and vibration response of FGM plate.

4.2.1 Vibration analysis of FGM plate

In Table 3, the frequency parameter of fully clamped square Ti–6Al–4V/Si$_3$N$_4$ FGM plate is presented for side to thickness ratio and volume fraction indexes (n). The influence of two micromechanics model (Mori–Tanaka and Voigt model) on the frequency parameter is also discussed in the results. The non-dimensional frequency parameter is assumed as $\left(\bar{\bar{\omega}} = \omega\left(a^2/h\right)\sqrt{\rho_c/E_c}\right)$. The material properties of the constituent material are $E_m = 105.7$ GPa, $\rho_m = 4429$ kg/m^3, $\upsilon_m = 0.298$ for Ti–6Al–4V, and $E_c = 322.27$ GPa, $\rho_c = 2370$ kg/m^3, $\upsilon_c = 0.25$ for Si$_3$N$_4$. It is perceived from the results that by increasing side to thickness ratio, the frequency parameter increases. It is also found that the frequency parameter decreases with increase in volume fraction index 'n'. It is evident from the results that Voigt and Mori–Tanaka models delivers same results for an isotropic plate ($n = 0$), whereas very small changes are seen for the rest of the values of volume fraction index 'n'. It is observed from the results that the maximum percentage difference between the two models is 4.23%.
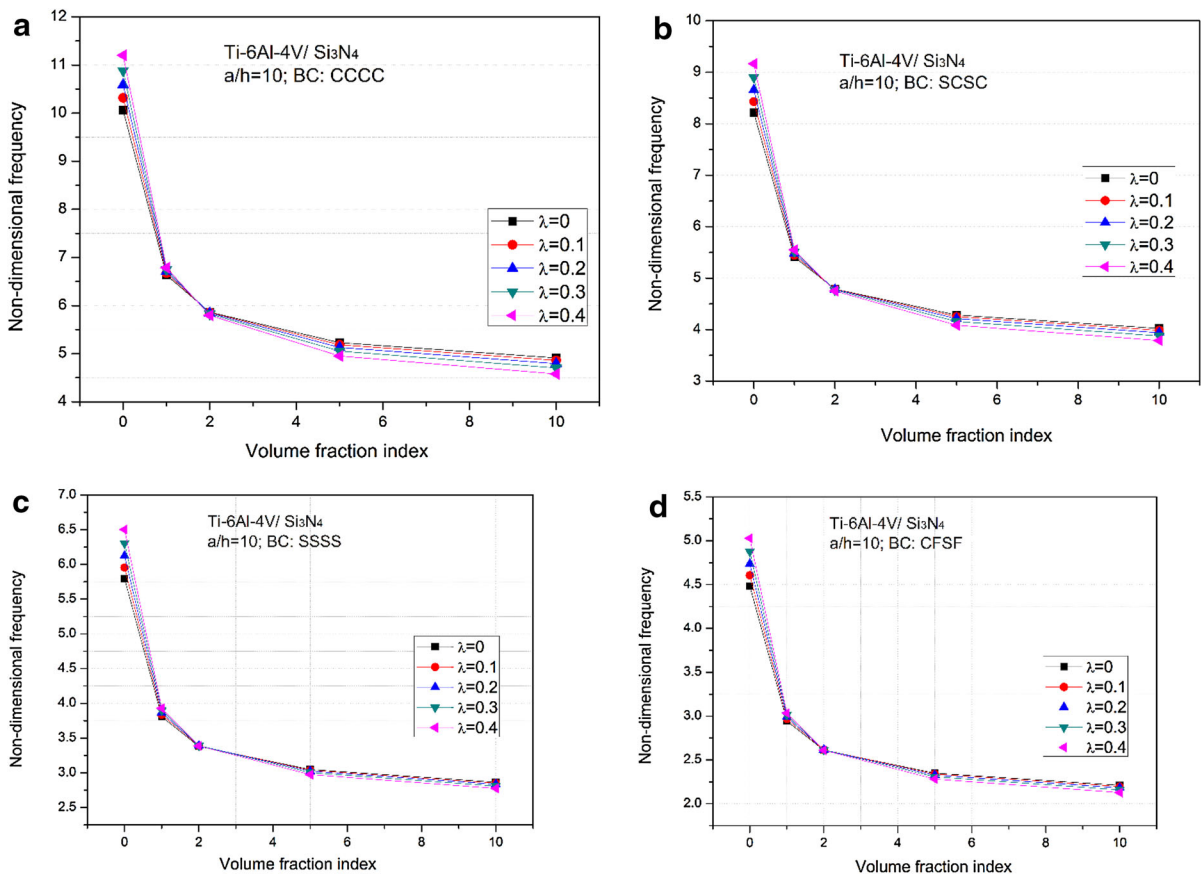
Fig. 7 Non-dimensional frequency versus volume fraction index for different porosity volume fraction (λ)

Tables 4, 5 and 6 show the effect of various side to thickness ratios and volume fraction index on the frequency parameter of SCSC, SSSS, and CFSF FGM plate respectively. This shows the consistent behavior as discussed in the former section. Again, the maximum percentage difference in the results obtained from two different homogenization techniques (Voigt and M–T) is 4.07%. It is notable that the Mori–Tanaka model slightly overpredicts the frequency ratio as compared to Voigt model. In the succeeding sections, only Voigt model is used to compute the effective material properties of FGM plate.

In Fig. 5a, the influence of aspect ratio (b/a) and volume fraction index 'n' on the frequency parameter of fully clamped FGM plate is shown. It is evident from the figure that the frequency parameter decreases with increases in aspect ratio and volume fraction index. Figure 5b–d present the variation of frequency parameter of FGM plate with aspect ratio for SCSC, SSSS, and CFSF boundary conditions respectively. It is observed form the results that for CCCC FGM plate, the frequency parameter decreases up to 33% when aspect ratio increases from 1 to 3, on the other hand, this reduction in the frequency parameter is

approximately 88% for CFSF FGM. Therefore, it can be concluded that the influence of aspect ratio is more on the plate having fewer boundary constraints.

Figure 6a–d represent the effect of porosity on the non-dimensional frequency parameter of CCCC, SCSC, SSSS, and CFSF FGM plate respectively. It is observed that the frequency increases as the porosity volume fraction (λ) increase for all the boundary conditions considered herewith. It is perceived that the range of percentage increment in frequency parameter is approximately 0.5–1.5% for $a/h = 5$, whereas this value is increased to nearly 3.8% for $a/h = 100$.

Hence, it is concluded that the thin plate is more sensitive to porosity as a comparison to the thick plate.

In Fig. 7a–d, the influence of porosity on the frequency parameter is demonstrated with the variation of volume fraction index for various boundary constraints. From the obtained results, it is noticed that the when the FGM plate is fully ceramic ($n = 0$), frequency parameter increases as the porosity volume fraction. But as the metal constituent increases ('n' increases from 1 to 10) in the FGM plate, frequency parameter decreases as the porosity volume fraction increases. It is apparent that the maximum change in
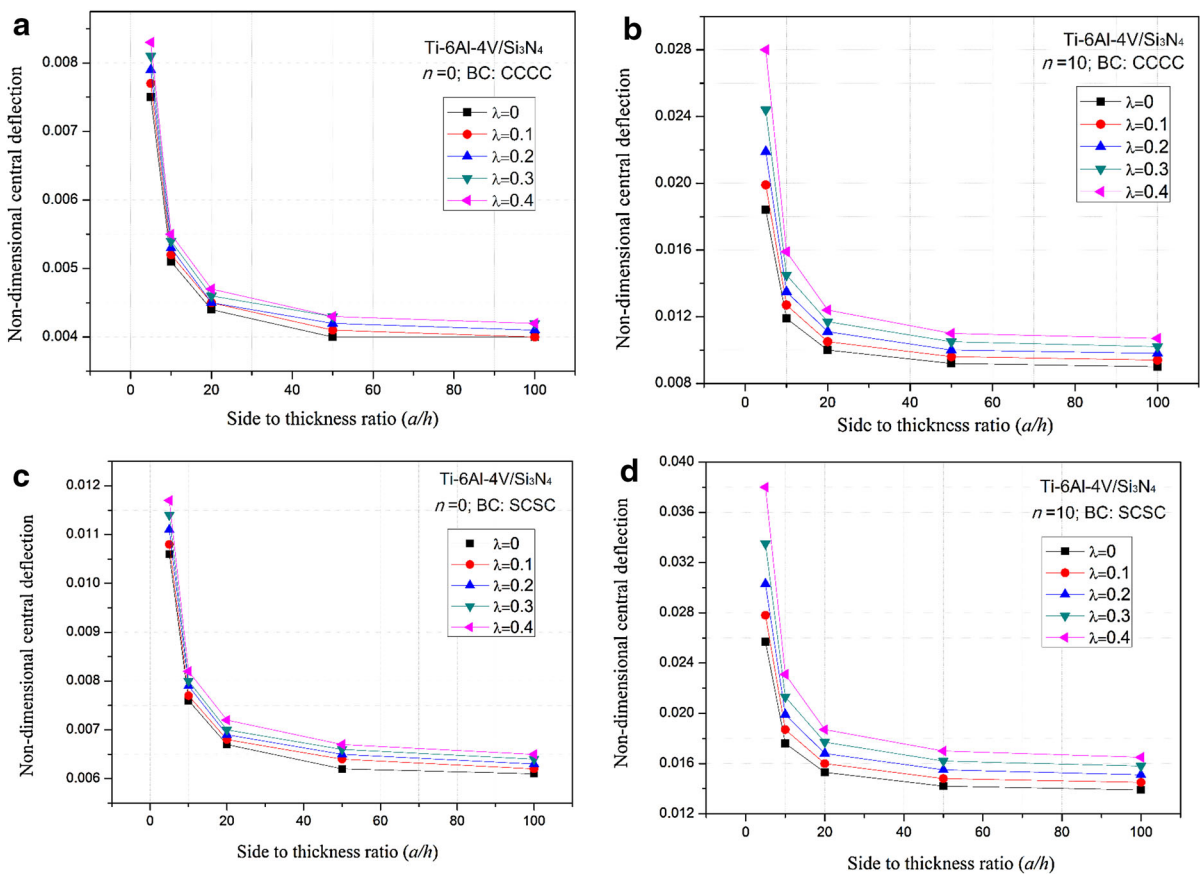
Fig. 8 Variation of central deflection with side to thickness ration and porosity volume fraction index (λ) for FGM plate ($n = 1$ and 10)
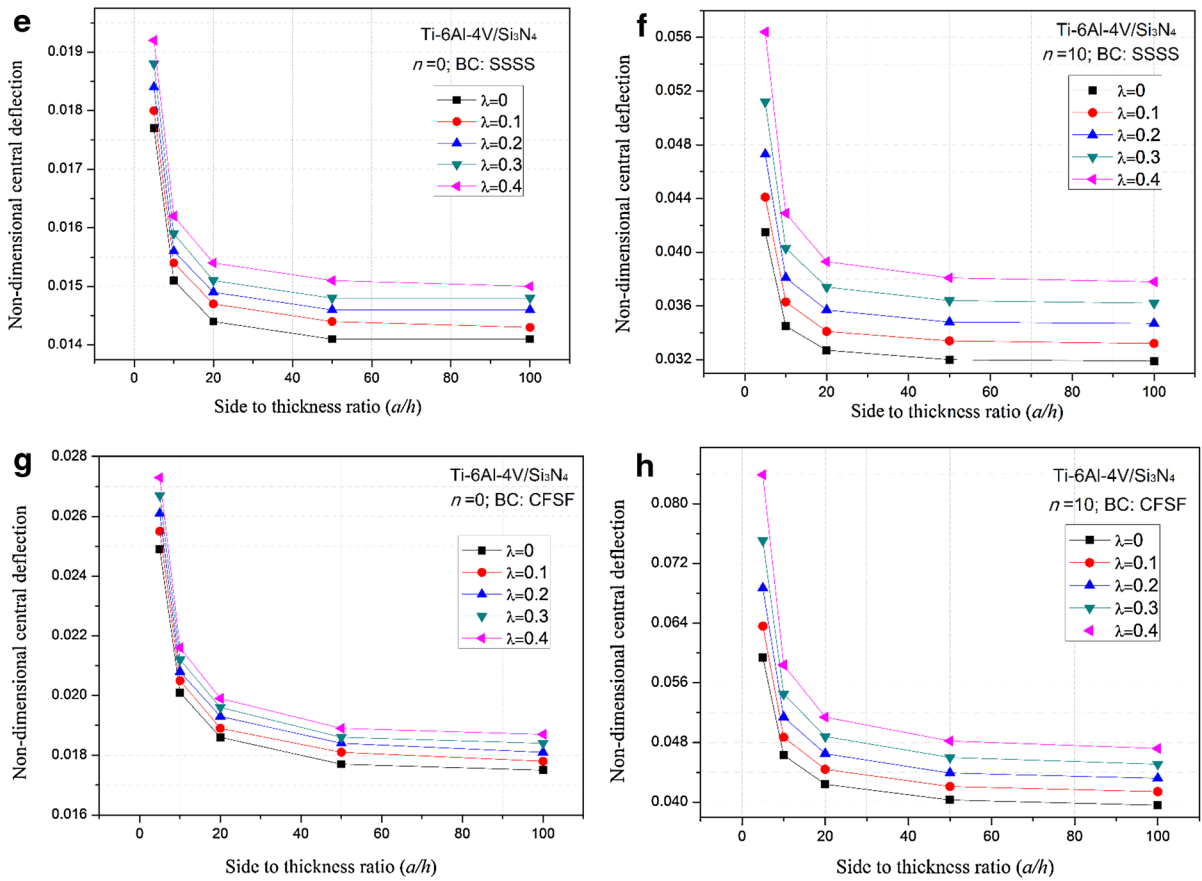
Fig. 8 continued

the frequency is approximately 11% due to porosity when 'n' is 0 but this value is nearly 6% of the higher value of 'n'.

4.2.2 Flexural response

In this section, the flexural response is performed for the FGM plate made of Ti–6Al–4V/Si$_3$N$_4$ with porosity. The transverse displacement *(w)*, thickness coordinate *(z)* and the pressure *(Q)* applied to the top surface of the plate are presented in nondimensionalized form as

$$\bar{w} = w/h, \quad Q = qa^4 / E_m h^4, \quad \bar{z} = z/h \qquad (23)$$

Figure 8a–b depicts the variation of non-dimensional central deflection of (Ti–6Al–4V/Si$_3$N$_4$) fully clamped FGM plate with side to thickness ratio and porosity volume fraction for $n = 0$ and 10. It is manifest from the results that the central deflection decreases with increase *a/h* ratio up to a certain limit
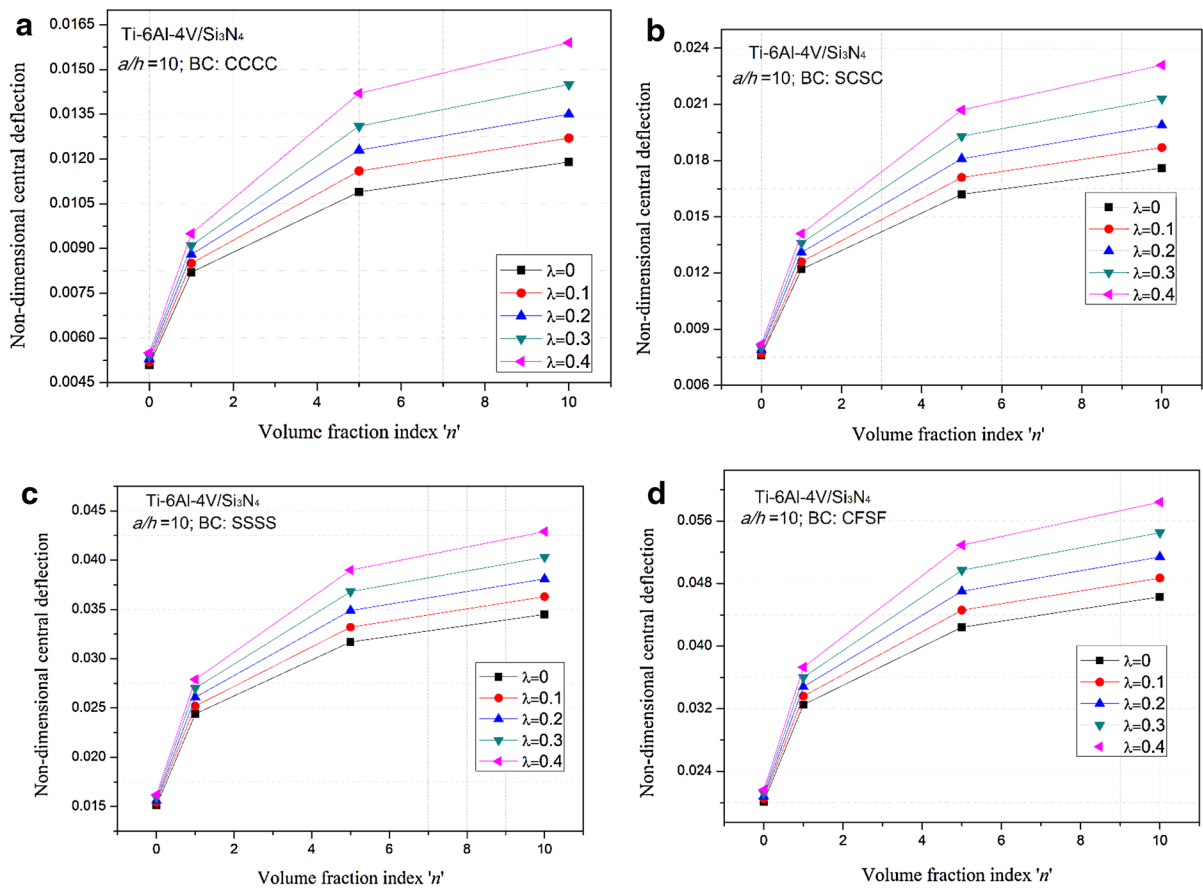
Fig. 9 Variation of central deflection with volume fraction index and porosity volume fraction (λ) for FGM plate

($a/h = 50$) beyond this no substantial change in the deflection occurs. It is also observed that the central deflection increases with porosity volume fraction (λ). In Fig. 8c–h, central deflection is plotted against the side to thickness ratio and porosity volume fraction with $n = 0$ and 10 for SCSC, SSSS, and CFSF boundary conditions respectively. In all the cases, the flexural response reflects the consistent behavior as discussed for Fig. 8a–b.

In Fig. 9a–d, the effect of porosity and volume fraction index on the central deflection of FGM plate is investigated for various boundary conditions. It is observed that the change in central deflection is ranged from 5 to 10% when porosity volume fraction increases from 0 to 0.4 for fully ceramic FGM plate ($n = 0$), whereas this percentage change is reduced to only 18–52% for the higher values of 'n'. Therefore, it is concluded that the flexural response is significantly

influenced by the porosity in the FGM plate having more volume fraction of ceramic.

5 Conclusions

The flexural and vibration response of functionally graded plate with porosity is analyzed using recently developed nonpolynomial higher-order shear and normal deformation theory to ensure its efficiency and applicability. This theory satisfies not only the shear stress-free boundary conditions at the top and bottom surfaces of the plate but also accommodate the thickness stretching effects. The new mathematical model is developed through the reformulation of the rule of mixture to incorporate the porosity phase in the material properties. Finite element formulation has been carried out using C^0 isoparametric element with 72 degrees of freedom per element. Several significant effects of volume fraction of porosity, volume fraction index, geometric configuration, homogenization techniques and boundary conditions on the flexural and vibration characteristics of FGM plate are investigated. The whole analysis concludes with some significant observations that are summarized as follows:

- Porosity volume fraction is an essential parameter in structural component design. The frequency increases as the porosity volume fraction increases.
- The effect of porosity is prominent in metal whereas its effect weakens as ceramic content in the FGM plate increases.
- The effect of porosity is perceptible in thin plates.
- The presence of porosity leads to increase the deflection in all the boundary conditions considered in the present study.

- Significant changes in deflection and frequency observed for $a/h < 50$, but for $a/h > 50$ no notable changes observed in deflection and frequency.

Appendix

Notation and description of various entities associated in mathematical modelling of structural kinematics

a, b, h	Length, width and thickness of the FGM plate	E	Effective Young's modulus
x, y, z	Cartesian coordinate	ρ	Effective mass density
u_o, v_o, w_b	Mid-plane displacements	υ	Poisson's ratio
w	Transverse displacement component	$[\mathbf{M}]$	Mass matrix
κ	Shape parameter	$[\mathbf{K}]$	Stiffness matrix
ε	Linear strain vector	ω	Natural frequency
V_c	Volume fraction of ceramic	$\bar{w}$	Central deflection
V_m	Volume fraction of metal	λ	Porosity volume fraction

$$[\mathcal{N}] = \begin{bmatrix} 1 & 0 & 0 & \Omega_1(z) & 0 & 0 & \Omega_2(z) & 0 \\ 0 & 1 & 0 & 0 & \Omega_1(z) & 0 & 0 & \Omega_2(z) \\ 0 & 0 & 1 & 0 & 0 & 0 & 0 & \Omega_3(z) \end{bmatrix}$$

$$\Omega_1(z) = -z,$$

$$\Omega_2(z) = \psi Sinh^{-1}\left(\frac{\kappa z}{h}\right) - \left(\frac{\kappa \psi}{h}\right),$$

$$\Omega_3(z) = \kappa Cosh^2\left(\frac{\kappa z}{h}\right)$$

$$[\mathbf{M}] = \begin{bmatrix} 1 & 0 & 0 & 0 & 0 & z & 0 & 0 & \Omega_2(z) & 0 & 0 & 0 & 0 & 0 & 0 & 0 \\ 0 & 1 & 0 & 0 & 0 & 0 & z & 0 & 0 & \Omega_2(z) & 0 & 0 & 0 & 0 & 0 & 0 \\ 0 & 0 & 0 & 0 & 0 & 0 & 0 & 0 & 0 & 0 & 0 & 0 & 0 & 0 & 0 & \Omega_3'(z) \\ 0 & 0 & 1 & 0 & 0 & 0 & 0 & 0 & 0 & 0 & 0 & \Omega_3(z) & 0 & \Omega_3'(z) & 0 & 0 \\ 0 & 0 & 0 & 1 & 0 & 0 & 0 & 0 & 0 & 0 & 0 & 0 & \Omega_3(z) & 0 & \Omega_3'(z) & 0 \\ 0 & 0 & 0 & 0 & 1 & 0 & 0 & Z & 0 & 0 & \Omega_2(z) & 0 & 0 & 0 & 0 & 0 \end{bmatrix}$$

References

Alipour, M.M., Shariyat, M., Shaban, M.: A semi-analytical solution for free vibration of variable thickness two-directional-functionally graded plates on elastic foundations. Int. J. Mech. Mater. Des. **6**, 293–304 (2010). doi:10.1007/s10999-010-9134-2

Ameur, M., Tounsi, A., Mechab, I., El Bedia, A.A.: A new trigonometric shear deformation theory for bending analysis of functionally graded plates resting on elastic foundations. KSCE J. Civ. Eng. **15**, 1405–1414 (2011). doi:10.1007/s12205-011-1361-z

Atmane, A.H., Tounsi, A., Bernard, F.: Effect of thickness stretching and porosity on mechanical response of a functionally graded beams resting on elastic foundations. Int. J. Mech. Mater. Des. (2015). doi:10.1007/s10999-015-9318-x

Atmane, H.A., Tounsi, A., Mechab, I., El Bedia, A.A.: Free vibration analysis of functionally graded plates resting on Winkler-Pasternak elastic foundations using a new shear deformation theory. Int. J. Mech. Mater. Des. **6**, 113–121 (2010). doi:10.1007/s10999-010-9110-x

Basset, A.B.: On the extension and flexure of cylindrical and spherical thin elastic shells. Philos. Trans. R. Soc. A Math. Phys. Eng. Sci. **181**, 433–480 (1890). doi:10.1098/rsta.1890.0007

Belabed, Z., Houari, M.S.A., Tounsi, A., Mahmoud, S.R.R., Beg, O.Anwar: An efficient and simple higher order shear and normal deformation theory for functionally graded material (FGM) plates. Compos. Part B Eng. **60**, 274–283 (2014). doi:10.1016/j.compositesb.2013.12.057

Benachour, A., Tahar, H.D., Atmane, H.A., Tounsi, A., Ahmed, M.S.: A four variable refined plate theory for free vibrations of functionally graded plates with arbitrary gradient. Compos. Part B Eng. **42**, 1386–1394 (2011). doi:10.1016/j.compositesb.2011.05.032

Carrera, E., Brischetto, S., Cinefra, M., Soave, M.: Effects of thickness stretching in functionally graded plates and shells. Compos. B Eng. **42**, 123–133 (2011). doi:10.1016/j.compositesb.2010.10.005

Chi, S.H., Chung, Y.L.: Mechanical behavior of functionally graded material plates under transverse load—Part I: analysis. Int. J. Solids Struct. **43**, 3657–3674 (2006). doi:10.1016/j.ijsolstr.2005.04.011

Ebrahimi, F., Zia, M.: Large amplitude nonlinear vibration analysis of functionally graded Timoshenko beams with porosities. Acta Astronaut. **116**, 117–125 (2015). doi:10.1016/j.actaastro.2015.06.014

Ferreira, A.J.M., Batra, R.C., Roque, C.M.C., Qian, L.F.F., Martins, P.A.L.S.: Static analysis of functionally graded plates using third-order shear deformation theory and a meshless method. Compos. Struct. **69**, 449–457 (2005). doi:10.1016/j.compstruct.2004.08.003

Gibson, L.J., Ashby, M.F., Karam, G.N., Wegst, U., Shercliff, H.R.: The mechanical properties of natural materials. II. Microstructures for mechanical efficiency. Proc. R. Soc. A Math. Phys. Eng. Sci. **450**, 141–162 (1995). doi:10.1098/rspa.1995.0076

Grover, N., Singh, B.N., Maiti, D.K.: Analytical and finite element modeling of laminated composite and sandwich plates: an assessment of a new shear deformation theory for free vibration response. Int. J. Mech. Sci. **67**, 89–99 (2013). doi:10.1016/j.ijmecsci.2012.12.010

Gupta, A., Talha, M.: Recent development in modeling and analysis of functionally graded materials and structures. Prog. Aerosp. Sci. **79**, 1–14 (2015). doi:10.1016/j.paerosci.2015.07.001

Gupta, A., Talha, M.: An assessment of a non-polynomial based higher order shear and normal deformation theory for vibration response of gradient plates with initial geometric imperfections. Compos. B **107**, 141–161 (2016). doi:10.1016/j.compositesb.2016.09.071

Gupta, A., Talha, M., Chaudhari, V.K.: Natural frequency of functionally graded plates resting on elastic foundation using finite element method. Procedia Technol. **23**, 163–170 (2016b). doi:10.1016/j.protcy.2016.03.013

Gupta, A., Talha, M., Seemann, W.: Free vibration and flexural response of functionally graded plates resting on Winkler-Pasternak elastic foundations using non-polynomial higher order shear and normal deformation theory. Mech. Adv. Mater. Struct. (2017). doi:10.1080/15376494.2017.1285459

Gupta, A., Talha, M., Singh, B.N.: Vibration characteristics of functionally graded material plate with various boundary constraints using higher order shear deformation theory. Compos. B Eng. **94**, 64–74 (2016a). doi:10.1016/j.compositesb.2016.03.006

Hadji, L., Atmane, H.A., Tounsi, A., Mechab, I., Addabedia, E.A.: Free vibration of functionally graded sandwich plates using four-variable refined plate theory. Appl. Math. Mech. (English Edition) **32**, 925–942 (2011). doi:10.1007/s10483-011-1470-9

Jha, D.K., Kant, T., Singh, R.K.: Free vibration response of functionally graded thick plates with shear and normal deformations effects. Compos. Struct. **96**, 799–823 (2013). doi:10.1016/j.compstruct.2012.09.034

Kant, T., Owen, D.R.J., Zienkiewicz, O.C.: A refined higher-order C o plate bending element. Comput. Struct. **15**, 177–183 (1982)

Karama, M., Afaq, K.S., Mistou, S.: A new theory for laminated composite plates. Proc. Inst. Mech. Eng. Part L: J Mater. Des. Appl. **223**, 53–62 (2009). doi:10.1243/14644207JMDA189

Kashtalyan, M.: Three-dimensional elasticity solution for bending of functionally graded rectangular plates. Eur. J. Mech. A/Solids **23**, 853–864 (2004). doi:10.1016/j.euromechsol.2004.04.002

Kirchhoff GR: Uber das gleichgewicht und die bewegung einer elastischen Scheibe. J Reine Angew Math (Crelle's J) **40**, 51–88 (1850)

Koiter, W.T.: A consistent first approximation in the general theory of thin elastic shells. In Proceedings of First Symposium on the Theory of Thin Elastic Shells. North-Holland, Amsterdam (1959)

Lal, A., Jagtap, K.R., Singh, B.N.: Stochastic nonlinear bending response of functionally graded material plate with random system properties in thermal environment. Int. J. Mech. Mater. Des. **8**, 149–167 (2012). doi:10.1007/s10999-012-9183-9

Levinson, M.: An accurate simple theory of statics and dynamics of elastic plates. Mech. Res. Commun. **7**, 343–350 (1980)

Lo, K.H., Christensen, R.M., Wu, E.M.: A high-order theory of plate deformation—part 2: laminated plates. J. Appl. Mech. **44**, 669 (1977)

Magnucka-Blandzi, E.: Non-linear analysis of dynamic stability of metal foam circular plate. J. Theor. Appl. Mech. **48**, 207–217 (2010)

Mantari, J.L., Guedes Soares, C.: A novel higher-order shear deformation theory with stretching effect for functionally graded plates. Compos. Part B Eng. **45**, 268–281 (2013). doi:10.1016/j.compositesb.2012.05.036

Mantari, J.L.L., Oktem, A.S.S., Guedes Soares, C.: Bending response of functionally graded plates by using a new higher order shear deformation theory. Compos Struct. **94**, 714–723 (2012). doi:10.1016/j.compstruct.2011.09.007

Matsunaga, H.: Stress analysis of functionally graded plates subjected to thermal and mechanical loadings. Compos. Struct. **87**, 344–357 (2009). doi:10.1016/j.compstruct.2008.02.002

Mechab, I., Mechab, B., Benaissa, S., Serier, B., Bachir Bouiadjra, B.: Free vibration analysis of FGM nanoplate with porosities resting on Winkler Pasternak elastic foundations based on two-variable refined plate theories. J. Braz. Soc. Mech. Sci. Eng. (2016). doi:10.1007/s40430-015-0482-6

Mindlin, R.D.: Influence of rotatory inertia and shear on flexural motions of isotropic, elastic plates. ASME J. Appl. Mech. **18**, 31–38 (1951)

Mojdehi, A.R., Darvizeh, A.: Three dimensional static and dynamic analysis of thick functionally graded plates by the meshless local Petrov–Galerkin (MLPG) method. Engineering Analysis with … **35**, 1168–1180 (2011)

Mori, T., Tanaka, K.: Average stress in matrix and average elastic energy of materials with misfitting inclusions. Acta Metall. **21**, 571–574 (1973). doi:10.1016/0001-6160(73)90064-3

Murthy, M. V. V.: An improved transverse shear deformation theory for laminated anisotropic plates. NASA Technical Paper 1903 (1981)

Nguyen, Tk: A higher-order hyperbolic shear deformation plate model for analysis of functionally graded materials. Int. J. Mech. Mater. Des. **11**, 203–219 (2015). doi:10.1007/s10999-014-9260-3

Pandya, B.N., Kant, T.: Finite element analysis of laminated composite plates using a higher-order displacement model. Compos. Sci. Technol. **32**, 137–155 (1988). doi:10.1016/0266-3538(88)90003-6

Prakash, T., Ganapathi, M.: Asymmetric flexural vibration and thermoelastic stability of FGM circular plates using finite element method. Compos. B Eng. **37**, 642–649 (2006). doi:10.1016/j.compositesb.2006.03.005

Qian, L.F., Batra, R.C., Chen, L.M.: Static and dynamic deformations of thick functionally graded elastic plates by using higher-order shear and normal deformable plate theory and meshless local Petrov-Galerkin method. Compos. B Eng. **35**, 685–697 (2004). doi:10.1016/j.compositesb.2004.02.004

Reddy, J.N.: A simple higher-order theory for laminated composite plates. J. Appl. Mech. **51**, 745 (1984). doi:10.1115/1.3167719

Reddy, J.N.: Analysis of functionally graded plates. Int. J. Numer. Meth. Eng. **47**, 663–684 (2000)

Reissner, E.: The effect of transverse shear deformation on the bending of elastic plates. ASME J. Appl. Mech. **12**, 68–77 (1945)

Soldatos, K.P.: A transverse shear deformation theory for homogeneous monoclinic plates. Acta Mech. **94**, 195–220 (1992). doi:10.1007/BF01176650

Talha, M., Singh, B.N.: Static response and free vibration analysis of FGM plates using higher order shear deformation theory. Appl. Math. Model. **34**, 3991–4011 (2010). doi:10.1016/j.apm.2010.03.034

Talha, M., Singh, B.N.: Thermo-mechanical buckling analysis of finite element modeled functionally graded ceramic-metal plates. Int. J. Appl. Mech. **3**, 867–880 (2011a). doi:10.1142/S1758825111001275

Talha, M., Singh, B.N.: Nonlinear mechanical bending of functionally graded material plates under transverse loads with various boundary conditions. Int. J. Model. Simul. Sci. Comput. **2**, 237–258 (2011b). doi:10.1142/S1793962311000451

Tamijani, A.Y., Kapania, R.K.: vibration analysis of curvilinearly-stiffened functionally graded plate using element free Galerkin method. Mech. Adv. Mater. Struct. **19**, 100–108 (2012). doi:10.1080/15376494.2011.572240

Thai, H.T., Choi, D.H.: Efficient higher-order shear deformation theories for bending and free vibration analyses of functionally graded plates. Arch. Appl. Mech. **83**, 1755–1771 (2013). doi:10.1007/s00419-013-0776-z

Thai, H.T., Kim, S.E.: A simple quasi-3D sinusoidal shear deformation theory for functionally graded plates. Compos. Struct. **99**, 172–180 (2013). doi:10.1016/j.compstruct.2012.11.030

Touratier, M.: An efficient standard plate theory. Int. J. Eng. Sci. **29**, 901–916 (1991)

Vaghefi, R., Baradaran, G.H., Koohkan, H.: Three-dimensional static analysis of thick functionally graded plates by using meshless local Petrov-Galerkin (MLPG) method. Eng. Anal. Boundary Elem. **34**, 564–573 (2010). doi:10.1016/j.enganabound.2010.01.005

Wattanasakulpong, N., Ungbhakorn, V.: Linear and nonlinear vibration analysis of elastically restrained ends FGM beams with porosities. Aerosp. Sci. Technol. **32**, 111–120 (2014). doi:10.1016/j.ast.2013.12.002

Wattanasakulpong, N., Prusty, B.G., Kelly, D.W., Hoffman, M: Free vibration analysis of layered functionally graded beams with experimental validation. Mater. Des. (1980–2015) **36** 182–190 (2012). doi:10.1016/j.matdes.2011.10.049

Wu, C.P., Chen, S.J., Chiu, K.H.: Three-dimensional static behavior of functionally graded magneto-electro-elastic plates using the modified Pagano method. Mech. Res. Commun. **37**, 54–60 (2010). doi:10.1016/j.mechrescom.2009.10.003

Xiang, S., Kang, G.: Static analysis of functionally graded plates by the various shear deformation theory. Compos. Struct. **99**, 224–230 (2013). doi:10.1016/j.compstruct.2012.11.021

Yahia, S.A., Atmane, H.A., Houari, M.S.A., Tounsi, A.: Wave propagation in functionally graded plates with porosities using various higher-order shear deformation plate theories. Struct. Eng. Mech. **53**, 1143–1165 (2015). doi:10.12989/sem.2015.53.6.1143

Zenkour, A.M.: A comprehensive analysis of functionally gra-
    ded sandwich plates: part 2-buckling and free vibration.
    Int. J. Solids Struct. **42**, 5243–5258 (2005). doi:10.1016/j.
    ijsolstr.2005.02.016

Zenkour, A.M.: Generalized shear deformation theory for
    bending analysis of functionally graded plates. Appl. Math.
    Model. **30**, 67–84 (2006). doi:10.1016/j.apm.2005.03.009

Zhu, P., Liew, K.M.: Free vibration analysis of moderately thick
    functionally graded plates by local Kriging meshless
    method. Compos. Struct. **93**, 2925–2944 (2011). doi:10.
    1016/j.compstruct.2011.05.011